Hindawi
Shock and Vibration
Volume 2020, Article ID 8859527, 17 pages
https://doi.org/10.1155/2020/8859527

Research Article

Damage Localization in a Building Structure during Seismic Excitation

Jesús Morales-Valdez,[1] **Luis Alvarez-Icaza**,[2] **and José A. Escobar**[2]

[1]*Cátedras CONACYT-CINVESTAV IPN, Av. Instituto Politécnico Nacional 2508 Gustavo A. Madero, México City 07360, Mexico*
[2]*Universidad Nacional Autónoma de México, 04510 Coyoacán, México City, Mexico*

Correspondence should be addressed to Jesús Morales-Valdez; jesus.moralesv@gmail.com

Received 25 April 2020; Revised 8 June 2020; Accepted 1 July 2020; Published 28 July 2020

Academic Editor: Matteo Strozzi

Aging of buildings during their service life has attracted the attention of researchers on structural health monitoring (SHM). This paper is related with detecting damage in building structures at the earliest possible stage during seismic activity to facilitate decision-making on evacuation before physical inspection is possible. For this, a simple method for damage assessment is introduced to identify the damage story of multistory buildings from acceleration measurements under a wave propagation approach. In this work, damage is assumed as reduction in shear wave velocities and changes in damping ratios that are directly related with stiffness loss. Most damage detection methods are off-line processes; this is not the case with this method. First, a real-time identification system is introduced to estimate the current parameters to be compared with nominal values to detect any changes in the characteristics that may indicate damage in the building. In addition, this identification system is robust to constant disturbances and measurement noise. The time needed to complete parameter identification is shorter compared to the typically wave method, and the damage assessment can keep up with the data flow in real time. Finally, using a robust threshold, postprocess of the compared signal is performed to find the location of the possible damage. The performance of the proposed method is demonstrated through experiments on a reduced-scale five-story building, showing the ability of the proposed method to improve early stage structural health monitoring.

1. Introduction

Structures like buildings are frequently exposed to various kinds of damages during their service life mainly due to the continuous deterioration caused by material degradation, corrosion, fatigue, and unexpected heavy loads induced by earthquakes and strong winds. In this sense, structural health monitoring (SHM) allows to track changes in the dynamic characteristics of the structural system for inspecting structure's integrity and detecting any probable structural damage. Most SHM methods in civil engineering are based on modal analysis, which studies global changes in natural frequencies and modal shapes [1, 2]. Under this idea, extensive reviews of vibration-based damage identification methods are presented in [3–5] and subsequently every 5 years since 2003. Recent reviews on vibration-based damage detection can be consulted in [6, 7]. A limitation of this group of methods is that they require exciting a building at high frequencies, condition that is not easy to achieve, and therefore, damage may go unnoticed. In the same research direction, an improved method to detect the location of the damage is the curvature mode shape proposed in [8, 9] that is more sensitive to stiffness loss and strain change based on a flexibility index [10]. Damage can be localized by comparing changes in displacement mode shapes. However, if the damage is distributed throughout the structure and a baseline measurement data set of the undamaged structure is not available, the algorithm performance may decrease as a damage indicator.

Other studies for structural health monitoring are developed around a pattern classification framework; a review of these methods is presented in [11]. For instance, Sohn and

Farrar and Nair and Kiremidjian [12, 13] provide a procedure for damage detection and localization in a mechanical system analyzing the measured structural-vibration response with autoregressive models (ARX) and autoregressive moving average (ARMA), respectively. The assumption is that when the structure is damaged, the error between a measured signal and that obtained from these two models increases; thus, changes in the coefficients of the autoregressive part of the model can indicate damage. Following this line, convolutional neural network is an algorithm that allows to realize damage diagnosis using image classification [14, 15]. Other applications can be found in [16] that are based on a machine learning perspective to detect the damage of a bridge pier. Like in [17], damage detection is carried out by using a support vector machine (SVM), and Grubbs' test method is adopted to delete the outliers for the SVM. An artificial bee colony (ABC) algorithm via modal and frequency analyses is presented in [18] to detect structural damages under different identify conditions such as grouping, noise effect, mode shape order, and sensor location and is also evaluated by several explicit test functions. Damage detection is treated as an optimization problem. Moreover, note that all previous pattern recognition methods demand large time histories from the undamaged structure and intensive data processing.

Some new techniques employ model-based methods assuming that a detailed well-correlated numerical model of the structure is available for damage identification. Among them, finite element (FE) model is typically employed to minimize the differences between analytical and experimental results and is usually proposed as an optimization problem that minimizes the discrepancy by adjusting the unknowns of the FE mode, employing finite element model updating (FEMU). An extensive bulk of research studies of structural dynamic model updating techniques based on direct and iterative techniques of FEMU can be found in [19, 20]. The authors highlight the current issues, applications, and observations for further advancements in the field. Following this line, Sehgal and Kumar [21] presented the theory and numerical application of a damped updating technique, which is based on response models and Derringer's function approach. Updating process is formulated as an optimization problem, wherein desirability functions are formulated, based on natural frequencies and modal assurance criterion (MAC) values. Similarly, in [22], the application of Derringer's function-based weighted model updating method for damage detection in a simulated cantilever beam structure is investigated. In this method, FEMU is treated as a multiobjective optimization problem, where the number of objectives needs to be defined in such a way as to reduce errors in responses predicted by the FE model. Maximization of an individual desirability function leads to minimization of error in the corresponding finite element response to which the individual desirability function is attached. Experimental validation of this technique can be found in [23], where structural dynamic model updating has been utilized in experimentally evaluating the extent of damage at six locations of a damaged cantilever beam structure. Accurate damage identification was successfully performed by evaluating percent reduction in flexural rigidity. Similarly, a damped updating method to identify damage as well as damping parameters in a structure under real conditions is presented in [24]. Novelty of the work corresponds to experimental validation of the desirability function-based multiobjective optimization approach to identify the structural damage as well as damping parameters accurately in the real-life structure. It is important to note that the success of finite element model updating depends heavily on the selection of updating parameters since an ill-conditioned numerical problem may produce an updated model that becomes unsatisfactory or unrealistic [25].

Recently, the wave propagation approach has become relevant as an alternative method to identify building local characteristics. The underlying hypothesis is that, after damage occurred, shear wave velocity of propagation within the damaged zone is reduced. In the same research direction, [26–28] presented different wave methods for structural health monitoring and discussed advantages and limitations of this approach. An extension of studies on pulse propagation in uniform and layered shear beams is presented in [29, 30], where system identification of a layered shear building model is developed by using a direct algorithm based on ray theory. Similarly, Rahmani and Todorovska [31, 32] presented system identification with a waveform inversion algorithm for characterizing the shear velocities in layered shear beam and torsional shaft models. Seismic records from a 54-story steel-frame building are analyzed, and from them, wave velocity is derived as a damage indicator. In [33, 34], a method is proposed to monitor changes in the velocity of wave propagation through the structure identified by a least squares fit of a Timoshenko beam model. The author reported that the wave method could be successfully applied to a damaged structure with very dispersed wave propagation, resulting from bending deformation, in the absence of significant soil-structure interaction effects. From report results, wave propagation methods are promising in practice due to their robustness when applied to real damaged structures and insensitivity to the effects of soil-structure interaction [35, 36]. One common characteristic of all the above methods under this approach is that the analysis is performed off-line. This allows data processing or filtering that is normally computationally intensive; however, it prevents real-time response to changes in structures' health condition.

This paper extends the results presented in [30–32], where the off-line estimation of wave velocities in a layered shear beam model is studied. Here, two important features are included: (i) a new parameterization of the identification system problem to estimate velocities and damping coefficient and (ii) a methodology to locate possible damage, which is based on comparing changes in the wave parameters, processing these changes, and assessing damage using appropriate thresholds. Although

the wave propagation approach can be applied at large and small scales, in this paper, an intermediate scale is proposed that focuses on the damage location at a story level. The method is applied to structures built with frames under the action of shear forces in one direction. The developed identification algorithm is intended for use to SHM systems to provide early alerts during seismic activity. Therefore, if a structure is not safe, this system identification facilitates decision-making on evacuation before physical inspection is possible. Such timely damage assessment will help to avoid endangering human lives and to prevent injuries caused by potential collapse of a weakened structure during shaking from aftershocks, as well as unnecessary evacuation and loss of function of important structures such as hospitals when damage is nonexistent. Moreover, real-time damage detection allows fast response, avoids data storage, and discards the use of off-line data processing for eliminating acceleration measurement bias. This last one is achieved by using linear integral filters (LIF), as in [37], which eliminate constant disturbances, attenuate measurement noise, and avoid wave dispersion. This last feature is convenient as there is evidence of dispersion in structural systems [32, 38]. The system identification uses the normalized least square algorithm (NLSA) with forgetting factor, which provides real-time estimation of current parameters in the discretized shear beam model in contrast with [33, 39]. Therefore, the contribution of this paper can be summarized as follows:

(i) Proposing an online identification system that allows to recover in real time the best possible set of parameters in the least square sense that minimizes the error between the real and predicted output. This approach avoids dealing directly with wave reflection, transmission, and dispersion, as in previous wave methods. Moreover, the parametric projection algorithm guarantees estimates with a physical sense.

(ii) Introducing a new parameterization for the identification system that improves estimations of wave parameters considering measurements from a specific story and its adjacent floors. This improves the precision of the estimated parameters compared with previous works. Moreover, the discrete shear beam model only requires two free parameters per floor in contrast with the discrete shear building model.

(iii) Reducing the time needed to complete the parameter identification in comparison with a typical wave propagation method, and allowing the damage assessment to keep up with the data flow in real time.

(iv) Providing a real-time damage detection algorithm that is easier to implement in comparison with other alternative methodologies already available in the literature. When there is damage, ratios between parameters of shear wave velocity and damping in two adjoining floors always change at the damaged story. When there is no damage, these ratios would not change with time. Moreover, the selected damage detection threshold is robust at certain close values.

The specimen used in this study is a five-story small-scale building, where first, shear wave velocities and damping coefficients are obtained when the structure is damage-free. Later, two different scenarios are presented. In the first one of them, damage is produced at the second story and in the second one, in the second and fifth floors. In both cases, damage is performed by reducing the cross section of the columns, which results in stiffness loss. The experimental setup allows to easily calculate both analytically and experimentally the new expected stiffness values, as this is a useful parameter to evaluate the estimated shear wave velocities and damping coefficient, because these last parameters cannot be experimentally measured. However, from the results published in [30], it is known that wave propagation methods are sensitive to a wide type of damages. Moreover, considering nominal and currently estimated parameters, a methodology to locate the damage is introduced. The most important challenge is in defining the threshold range for damage detection, which was determined using the data collected in the tests to find the maximum change level. This allows us to calculate the standard deviation that each parameter may suffer.

This paper is organized as follows: the employed mathematical model is briefly presented in Section 2, and the real-time system identification design is presented in Section 3. The damage location methodology is described in Section 4, while experimental results are presented in Section 5. Finally, concluding remarks are presented in Section 6.

2. Mathematical Model of the Building

The dynamics of a multidegree-of-freedom (MDOF) building structure seismically excited is modeled employing a one-dimensional wave equation with Kelvin damping to study the wave propagation characteristics. The model and proper boundary conditions are [37]

$$\frac{\partial^2 u_i}{\partial t^2} = \beta_i^2 \frac{\partial^2 u_i}{\partial y^2} + \eta_i^2 \frac{\partial^2 \dot{u}_i}{\partial y^2}, \tag{1}$$

$$u(y,0) = 0, \quad 0 \le y \le H, \tag{2a}$$

$$\dot{u}(y,0) = 0, \quad 0 \le y \le H, \tag{2b}$$

$$\ddot{u}(0,t) = \ddot{u}_g, \quad 0 < t, \tag{2c}$$

$$\frac{\mu}{\partial y} \frac{\partial u}{\partial y}(H,t) = 0, \quad 0 < t, \tag{2d}$$

where β is the shear wave velocity, η is a constant proportional to damping in the structure, and μ is the shear module, whereas u and $\dot{u}$ are signals of displacement and

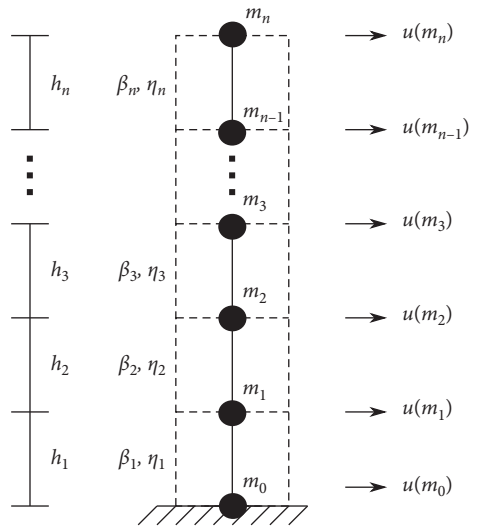

Figure 1: Discrete shear beam.

velocity, and u_g is the ground motion. Furthermore, according to equations (2a–2d), the following is assumed.

2.1. Remarks

(1) The building is initially at rest according to equations 2a and 2b

(2) Only the base of the structure is excited during seismic activity, see equation (2c)

(3) The building is stress-free at the roof in accordance with equation (2d)

(4) From equation (1), the shear building model can be treated as an elastic continuous shear beam, and thus, wave propagation effects can be studied and used as indicators of structural health

In order to propose a real-time identification system, the continuous shear beam model is discretized in points that coincide with instrumented stories. Therefore, different shear wave velocities and damping coefficients are produced, as shown in Figure 1. Discretization is carried out employing three-point central-difference approximation for stories 1 to $(n-1)$ and a first-order backward approximation for the remaining ones. Moreover, in order to improve discretization accuracy, the shear wave velocity and damping coefficient at each point are obtained with the average values of the nearest points, i.e.,

$$\beta^2(m_0) = \beta_1^2, \beta^2(m_1) = \frac{\beta_1^2 + \beta_2^2}{2}, \ldots, \beta^2(m_{n-1}) = \frac{\beta_{n-1}^2 + \beta_n^2}{2}, \beta^2(m_n) = \beta_n^2, \tag{3}$$

$$\eta^2(m_0) = \eta_1^2, \eta^2(m_1) = \frac{\eta_1^2 + \eta_2^2}{2}, \ldots, \eta^2(m_{n-1}) = \frac{\eta_{n-1}^2 + \eta_n^2}{2}, \eta^2(m_n) = \beta_n^2, \tag{4}$$

which will induce a different parameterization than the one presented in [38].

Furthermore, the resulting state matrix is expanded to use the acceleration measurement $\ddot{u}_g$ as the excitation signal, which is applied only at the Dirichlet boundary condition, in contrast to shear building models, where excitation is applied to all stories at the same time [40]. Eventually, the new ordinary differential and algebraic system equations have the possibility to be solved on real time [41]. Therefore, wave equation (1) is approximated by

$$\ddot{u} = \beta_M^2 \Lambda u + \eta_M^2 \Lambda \dot{u} + b\ddot{u}_g, \tag{5}$$

where

$$\beta_M^2\Lambda = \frac{1}{\Delta h^2}\begin{bmatrix} 0 & 0 & 0 & 0 & 0 & \cdots & 0 \\ \beta_1^2 & -2\dfrac{\beta_1^2+\beta_2^2}{2} & \dfrac{\beta_2^2+\beta_3^2}{2} & 0 & 0 & \cdots & 0 \\ 0 & \dfrac{\beta_1^2+\beta_2^2}{2} & -2\dfrac{\beta_2^2+\beta_3^2}{2} & \dfrac{\beta_3^2+\beta_4^2}{2} & 0 & \cdots & 0 \\ 0 & 0 & \dfrac{\beta_2^2+\beta_3^2}{2} & -2\dfrac{\beta_3^2+\beta_4^2}{2} & \dfrac{\beta_4^2+\beta_5^2}{2} & \cdots & 0 \\ \vdots & \vdots & \vdots & \ddots & \ddots & \ddots & \vdots \\ 0 & 0 & 0 & \cdots & \dfrac{\beta_{n-2}^2+\beta_{n-1}^2}{2} & -2\dfrac{\beta_{n-1}^2+\beta_n^2}{2} & \beta_n^2 \\ 0 & 0 & 0 & \cdots & 0 & \dfrac{\beta_{n-1}^2+\beta_n^2}{2} & -\beta_n^2 \end{bmatrix} \in \mathscr{R}^{p\times p}, \tag{6}$$

$$\eta_M^2\Lambda = \frac{1}{\Delta h^2}\begin{bmatrix} 0 & 0 & 0 & 0 & 0 & \cdots & 0 \\ \eta_1^2 & -2\dfrac{\eta_1^2+\eta_2^2}{2} & \dfrac{\eta_2^2+\eta_3^2}{2} & 0 & 0 & \cdots & 0 \\ 0 & \dfrac{\eta_1^2+\eta_2^2}{2} & -2\dfrac{\eta_2^2+\eta_3^2}{2} & \dfrac{\eta_3^2+\eta_4^2}{2} & 0 & \cdots & 0 \\ 0 & 0 & \dfrac{\eta_2^2+\eta_3^2}{2} & -2\dfrac{\eta_3^2+\eta_4^2}{2} & \dfrac{\eta_4^2+\eta_5^2}{2} & \cdots & 0 \\ \vdots & \vdots & \vdots & \ddots & \ddots & \ddots & \vdots \\ 0 & 0 & 0 & \cdots & \dfrac{\eta_{n-2}^2+\eta_{n-1}^2}{2} & -2\dfrac{\eta_{n-1}^2+\eta_n^2}{2} & \eta_n^2 \\ 0 & 0 & 0 & \cdots & 0 & \dfrac{\eta_{n-1}^2+\eta_n^2}{2} & -\eta_n^2 \end{bmatrix} \in \mathscr{R}^{p\times p}, \tag{7}$$

$$\begin{aligned} b &= [1,0,0,\ldots,0,0]^T, \in \mathscr{R}^{p\times 1}, \\ u &= \left[u_0, u_1, u_2, \ldots, u_{n-1}, u_n\right]^T, \in \mathscr{R}^{p\times 1}, \\ \dot{u} &= \left[\dot{u}_0, \dot{u}_1, \dot{u}_2, \ldots, \dot{u}_{n-1}, \dot{u}_n\right]^T, \in \mathscr{R}^{p\times 1}, \\ \ddot{u} &= \left[\ddot{u}_0, \ddot{u}_1, \ddot{u}_2, \ldots, \ddot{u}_{n-1}, \ddot{u}_n\right]^T, \in \mathscr{R}^{p\times 1}, \end{aligned} \tag{8}$$

with $p = (n+1)$; n is the total number of floors. Moreover, defining

$$\beta_{1*}^2 = \beta_1^2, \beta_{2*}^2 = \frac{\beta_1^2 + \beta_2^2}{2}, \ldots, \beta_{n-1*}^2 = \frac{\beta_{n-2}^2 + \beta_{n-1}^2}{2}, \beta_{n*}^2 = \frac{\beta_{n-1}^2 + \beta_n^2}{2}, \tag{9}$$

$$\eta_{1*}^2 = \eta_1^2, \eta_{2*}^2 = \frac{\eta_1^2 + \eta_2^2}{2}, \ldots, \eta_{n-1*}^2 = \frac{\eta_{n-2}^2 + \eta_{n-1}^2}{2}, \eta_{n*}^2 = \frac{\eta_{n-1}^2 + \eta_n^2}{2}, \tag{10}$$

then β_M^2 and η_M^2 are rewritten as

$$\beta_{M*}^2\Lambda = \frac{1}{\Delta h^2}\begin{bmatrix} 0 & 0 & 0 & 0 & 0 & \cdots & 0 \\ \beta_{1*}^2 & -2\beta_{2*}^2 & \beta_{3*}^2 & 0 & 0 & \cdots & 0 \\ 0 & \beta_{2*}^2 & -2\beta_{3*}^2 & \beta_{4*}^2 & 0 & \cdots & 0 \\ 0 & 0 & \beta_{3*}^2 & -2\beta_{4*}^2 & \beta_{5*}^2 & \cdots & 0 \\ \vdots & \vdots & \vdots & \ddots & \ddots & \ddots & \vdots \\ 0 & 0 & 0 & \cdots & \beta_{n-1*}^2 & -2\beta_{n*}^2 & \beta_*^2 \\ 0 & 0 & 0 & \cdots & 0 & \beta_{n*}^2 & -\beta_*^2 \end{bmatrix} \in \mathscr{R}^{p\times p}, \tag{11}$$

with

$$\beta_*^2 = 2\left[\beta_{5*}^2 - \beta_{4*}^2 + \beta_{3*}^2 - \beta_{2*}^2 + \frac{\beta_{1*}^2}{2}\right], \tag{12}$$

$$\eta_{M*}^2\Lambda = \frac{1}{\Delta h^2}\begin{bmatrix} 0 & 0 & 0 & 0 & 0 & \cdots & 0 \\ \eta_{1*}^2 & -\eta\beta_{2*}^2 & \eta_{3*}^2 & 0 & 0 & \cdots & 0 \\ 0 & \eta_{2*}^2 & -2\eta_{3*}^2 & \eta_{4*}^2 & 0 & \cdots & 0 \\ 0 & 0 & \eta_{3*}^2 & -2\eta_{4*}^2 & \eta_{5*}^2 & \cdots & 0 \\ \vdots & \vdots & \vdots & \ddots & \ddots & \ddots & \vdots \\ 0 & 0 & 0 & \cdots & \eta_{n-1*}^2 & -2\eta_{n*}^2 & \eta_*^2 \\ 0 & 0 & 0 & \cdots & 0 & \eta_{n*}^2 & -\eta_*^2 \end{bmatrix} \in \mathscr{R}^{p\times p}, \tag{13}$$

with

$$\eta_*^2 = 2\left[\eta_{5*}^2 - \eta_{4*}^2 + \eta_{3*}^2 - \eta_{2*}^2 + \frac{\eta_{1*}^2}{2}\right]. \tag{14}$$

However, equation (12) can be rewritten as $\Lambda\beta_{M+}^2$, i.e.,

$$\Lambda = \frac{1}{\Delta h^2}\begin{bmatrix} 0 & 0 & 0 & 0 & \cdots & 0 \\ 1 & -2 & 1 & 0 & \cdots & 0 \\ 0 & 1 & -2 & 1 & \cdots & 0 \\ \vdots & \vdots & \ddots & \ddots & \ddots & \vdots \\ 0 & 0 & \cdots & 1 & -2 & 1 \\ 0 & 0 & \cdots & 0 & 1 & -2 \end{bmatrix},$$

$$\beta_{M+}^2 = \begin{bmatrix} 0 & 0 & 0 & 0 & \cdots & 0 \\ 0 & \beta_{1*}^2 & 0 & 0 & \cdots & 0 \\ 0 & 0 & \beta_{2*}^2 & 0 & \cdots & 0 \\ \vdots & \vdots & \ddots & \ddots & \ddots & \vdots \\ 0 & 0 & \cdots & 0 & \beta_{n-1*}^2 & 0 \\ 0 & 0 & \cdots & 0 & 0 & \beta_{n*}^2 \end{bmatrix}. \tag{15}$$

Similarly, $\eta_{M+}^2 = \mathrm{diag}[0, \eta_{1*}^2, \eta_{2*}^2, \eta_{3*}^2, \ldots, \eta_{n*}^2]$.

On the contrary, $\Delta h = H/(n+1)$, where H is the building height. Matrices $\Lambda \in \mathscr{R}^{p\times p}$ and $b \in \mathscr{R}^{p\times 1}$ are the result of discretization, and they are related to the number of floors of the building. Considering that $\ddot{u}_0 = \ddot{u}_g$, the acceleration measurement at the boundary condition is available and equivalent to seismic action. Similarly, the displacement and velocity of the basement are denoted by u_0, and $\dot{u}_0$, respectively, while the remaining $u_i, \dot{u}_i$, and $\ddot{u}_i$ with $i = 1, 2, \ldots, n$ are the absolute displacements, velocities, and accelerations of each floor. Therefore, equation (5) does not need a coordinate transformation to be solved compared with other works [42]. Additionally, defining $\dot{u} = v$ allows expressing equation (5) in the space form as

$$\dot{x} = \mathscr{A}x + \mathscr{B}\ddot{u}_g, \tag{16}$$

with

$$x = \begin{bmatrix} \dot{u} \\ \dot{v} \end{bmatrix},$$

$$\mathscr{A} = \begin{bmatrix} 0_{pxp} & I_{pxp} \\ \beta_{M*}^2 & \eta_{M*}^2 \end{bmatrix}, \tag{17}$$

$$\mathscr{B} = \begin{bmatrix} 0_{px1} \\ b \end{bmatrix},$$

whose output equation is given by

$$z_m = \left(\ddot{u} - b\ddot{u}_g\right) = \left[\beta_{M*}^2\Lambda,\ \eta_{M*}^2\Lambda\right][u\ v]^T, \tag{18}$$

where $0_{p\times p}$ and $I_{p\times p}$ denote, respectively, the null and identity matrices of size $(p \times p)$.

3. System Identification

Defining $\lambda u = \psi$ and $\lambda \dot{u} = \dot{\psi}$, equation (18) is rearranged in a suitable form for identification:

$$z_m = \psi \beta_V^2 + \dot{\psi} \eta_V^2, \quad \text{with } z_m = \left(\ddot{u} - b\ddot{u}_g\right), \tag{19}$$

where elements of diagonal matrices β_{M+}^2 and η_{M+}^2 are used as elements in vectors β_V^2 and $\eta_V^2 \in \mathscr{R}^{p\times 1}$; matrices $\dot{\psi} \in \mathscr{R}^{p\times p}$ and vectors $\beta_V^2 = \Theta_\beta$, $\eta_V^2 = \Theta_\eta$ are defined as

$$\Theta_\beta = \beta_V^2$$

$$\psi = \frac{1}{\Delta h^2}\begin{bmatrix} 0 & 0 & 0 & 0 & 0 & \cdots & 0 \\ u_0 & -2u_1 & u_2 & 0 & 0 & \cdots & 0 \\ 0 & u_1 & -2u_2 & u_3 & 0 & \cdots & 0 \\ \vdots & \vdots & \vdots & \ddots & \ddots & \ddots & \vdots \\ 0 & 0 & 0 & \cdots & u_{n-2} & u_{n-1} & u_n \\ 0 & 0 & 0 & \cdots & 0 & u_{n-1} & -u_n \end{bmatrix}. \tag{20}$$

Hence, equation (19) is now of the form

$$z_m = \psi \Theta_\beta + \dot{\psi} \Theta_\eta. \tag{21}$$

However, equation (21) still depends on the nonmeasurable position and velocity signal contained in vectors ψ and $\dot{\psi}$ because displacement and velocity cannot be directly measured during seismic excitation. To overcome this problem, the following procedure is introduced. First, the model (21) is expressed in the frequency domain using the Laplace transform:

$$Z_m(s) = \Psi(s)\Theta_\beta + s\Psi(s)\Theta_\eta, \tag{22}$$

where $Z_m(s) = (\mathscr{L}[\ddot{u}] + \mathscr{L}[\ddot{u}]_g)$. Now, deriving three times equation (22), constant disturbances are removed, producing

$$s^3 Z(s) = s^3 \Psi(s)\Theta_\beta + s^4 \Psi(s)\Theta_\eta, \tag{23}$$

$$s^3 Z(s) = \mathscr{L}[\ddot{\psi}]\Theta_\beta + s^{2\mathscr{L}}[\ddot{\psi}]\Theta_\eta, \tag{24}$$

where $\ddot{\psi}$ is given by

$$\ddot{\psi} = \begin{bmatrix} 0 & 0 & 0 & 0 & 0 & \cdots & 0 \\ \ddot{u}_0 & -2\ddot{u}_1 & \ddot{u}_2 & 0 & 0 & \cdots & 0 \\ 0 & \ddot{u}_1 & -2\ddot{u}_2 & \ddot{u}_3 & 0 & \cdots & 0 \\ \vdots & \vdots & \vdots & \ddots & \ddots & \ddots & \vdots \\ 0 & 0 & 0 & \cdots & \ddot{u}_{n-2} & -2\ddot{u}_{n-1} & \ddot{u}_n \\ 0 & 0 & 0 & \cdots & 0 & \ddot{u}_{n-1} & -\ddot{u}_n \end{bmatrix}. \tag{25}$$

Note that while equation (22) depends on nonmeasurable signals, equation (24) depends only on measurable acceleration signals. Furthermore, (24) can be written in the time domain as

$$z_m^{(3)} = \psi^{(3)}\Theta_\beta + \psi^{(4)}\Theta_\eta, \tag{26}$$

where the superscript represents the j-th time derivative of the corresponding variable. Moreover, considering that acceleration signals are contaminated with offset and measurement noise, linear filter integrals (LIF) are introduced to eliminate this constant disturbance and to attenuate measurement noise [42]. This technique overcomes limitations that affect the performance of numerical integrators, as it is the case with bias and amplification of low-frequency noise. LIF is defined by the operator

$$I_q\{\phi(t)\} = \frac{1}{\delta^q}\int_{t-\delta}^{t}\int_{\tau_1-\delta}^{\tau_1}\cdots\int_{\tau_{q-1}-\delta}^{\tau_{q-1}}\phi\left(\tau_q\right)d\tau_q\cdots d\tau_1, \tag{27}$$

where q is the number of integrations over finite time intervals of signal $\phi(t)$. The time interval, $\delta \in \mathscr{R}^1$, is defined by the size of the moving window as

$$\delta = \overline{n}T_s, \tag{28}$$

where T_s is the sampling period and $\overline{n} > 0$ determines the length of the time integration window, which must be properly selected by making the system bandwidth and the filter cutoff frequencies to coincide. Applying the LIF operator $I_5[\cdot]$ to both sides of equation (26), which corresponds to the fifth-order low-pass filter, yields terms depending on the measured variables $\ddot{u}$ and z_m, i.e.,

$$\Xi(t) = \Upsilon_\beta(t)\Theta_\beta + \Upsilon_\eta(t)\Theta_\eta, \tag{29}$$

$$\Xi(t) = \frac{\vartheta}{\delta^3 I_2}\left\{\sum_{j=0}^{3}\frac{3}{j}(-1)^j z(t-j\delta)\right\}, \tag{30}$$

$$\Upsilon_\beta(t) = \frac{\vartheta}{\delta}I_4\left\{\sum_{j=0}^{1}\frac{1}{j}(-1)^j\ddot{\psi}(t-j\delta)\right\}, \tag{31}$$

$$\Upsilon_\eta(t) = \frac{\vartheta}{\delta^2}I_3\left\{\sum_{j=0}^{2}\frac{2}{j}(-1)^j\ddot{\psi}(t-j\delta)\right\}. \tag{32}$$

where

Thus, $\Xi \in \mathscr{R}^{p\times 1}$, Υ_β and $\Upsilon_\eta \in \mathscr{R}^{p\times p}$, n/j is the binomial coefficient, and finally, $\vartheta \in \mathscr{R}^+$ is a degree of freedom to normalize the amplitude of the filtered signals. From equation (29), the system output is parameterized as

$$\Xi(t) = \Upsilon(t), \tag{33}$$

where $\Theta = [\Theta_\beta^T, \Theta_\eta^T]^T \in \mathscr{R}^{2p\times 1}$ is a vector containing the real parameters of the system that will be estimated with the normalized least square algorithm (NLSA) and $\Upsilon = [\Upsilon_\beta, \Upsilon_\eta] \in \mathscr{R}^{p\times 2p}$ is the regressor matrix formed by filtered acceleration signals.

4. Damage Location Methodology

In this section, a two-stage damage location methodology is described. First, the parametric estimation algorithm developed is presented; then, once the current parameters that characterize the damage behavior are recovered, they are

compared with nominal parameters, and a damage location algorithm (DLA) is developed.

4.1. Parameter Estimation. Let $\widehat{\Theta} = [\widehat{\Theta}_\beta^T, \widehat{\Theta}_\eta^T]^T$ be the vector containing estimated parameters in equation (33) which are identified by using the normalized least square algorithm (NLSA) with forgetting factor given by equations (34 and 35) [43]:

$$\dot{P} = \alpha P - \frac{P\Upsilon^T \Upsilon P}{m^2}, \tag{34}$$

$$\dot{\widehat{\Theta}} = P\Upsilon^T, \tag{35}$$

where α is the forgetting factor, P is the covariance matrix, with $P = P^T > 0 \in \mathscr{R}^{2p\times 2p}$, $P(0) > 0$, $1 > \alpha \geq 0 \in \mathscr{R}^+$, and $m^2 = 1 + \Upsilon\Upsilon^T$, which satisfies $\Upsilon/m \in \mathscr{L}_\infty$ and assures that the normalized estimated error tends to zero, i.e.,

$$\varepsilon = \frac{\Xi - \widehat{\Xi}}{m^2} \longrightarrow 0 \quad \text{when } t \longrightarrow \infty. \tag{36}$$

Moreover, NLSA is improved using a parameter projection scheme that ensures only positive estimates and is defined by

$$\widehat{\Theta}_{\beta i+}(t) = \widehat{\Theta}_{\beta i}(t) + \left(\varsigma_1 - \widehat{\Theta}_{\beta i}(t)\right)\left(\frac{1}{2} - \frac{\chi_1 \widehat{\Theta}_{\beta i}(t)}{2\sqrt{\left(\chi_1 \widehat{\Theta}_{\beta i}(t)\right)^2 + e^2}}\right), \tag{37}$$

$$\widehat{\Theta}_{\eta i+}(t) = \widehat{\Theta}_{\eta i}(t) + \left(\varsigma_2 - \widehat{\Theta}_{\eta i}(t)\right)\left(\frac{1}{2} - \frac{\chi_2 \widehat{\Theta}_{\eta i}(t)}{2\sqrt{\left(\chi_2 \widehat{\Theta}_{\eta i}(t)\right)^2 + e^2}}\right), \tag{38}$$

where $\widehat{\Theta}_{\beta i+}(t)$ and $\widehat{\Theta}_{\eta i+}(t)$ are the projected estimates of $\Theta_{\beta i}$ and $\Theta_{\eta i}$, respectively, with $i = 0, 1, 2, \ldots, n$, $\varsigma_1 = 0.0001$ and $\varsigma_2 = 0.0001$ are the lower bounds for estimated parameters, whereas $\chi_1 = 500$ and $\chi_2 = 500$ allow to improve the estimation, and finally, $e = 0.05$. Note that $e > 0$ produce an approximation of the sign function, e.g.,

$$\operatorname{sign}\left(\widehat{\Theta}_i(t)\right) \approx \frac{\chi_1 \widehat{\Theta}_i(t)}{\sqrt{\left(\chi_1 \widehat{\Theta}_i(t)\right)^2 + e^2}}, \tag{39}$$

which allows to assume in equation (37) that $\widehat{\Theta}_{\beta i+}(t) \approx \varsigma_i$ when $\widehat{\Theta}_{\beta i}(t) < 0$; moreover, $\widehat{\Theta}_{\beta i+}(t) \approx \widehat{\Theta}_{\beta i}(t)$ when $\widehat{\Theta}_{\beta i}(t) > \varsigma_i$. Similar conditions apply to $\widehat{\Theta}_{\eta i}(t)$, ensuring that $\widehat{\Theta}_i(t) = [\widehat{\Theta}_{\beta i+}^T(t), \widehat{\Theta}_{\eta i+}^T(t)]^T$ always lie within $[\varsigma, \Theta]$, as shown in Figure 2. Therefore,

$$\begin{aligned} \widehat{\Theta}_{\beta+}(t) &= \left[0, \widehat{\Theta}_{\beta 1+}(t), \widehat{\Theta}_{\beta 2+}(t), \ldots, \widehat{\Theta}_{\beta n+}(t)\right]^T, \\ \widehat{\Theta}_{\eta+}(t) &= \left[0, \widehat{\Theta}_{\eta 1+}(t), \Theta_{\eta 2+}(t), \ldots, \widehat{\Theta}_{\eta m+}(t)\right]^T. \end{aligned} \tag{40}$$

Moreover, projected estimates in (37 and 38) have the advantage to be continuously differentiable functions, a useful feature for assuring that the estimation is stable (see Appendix A).

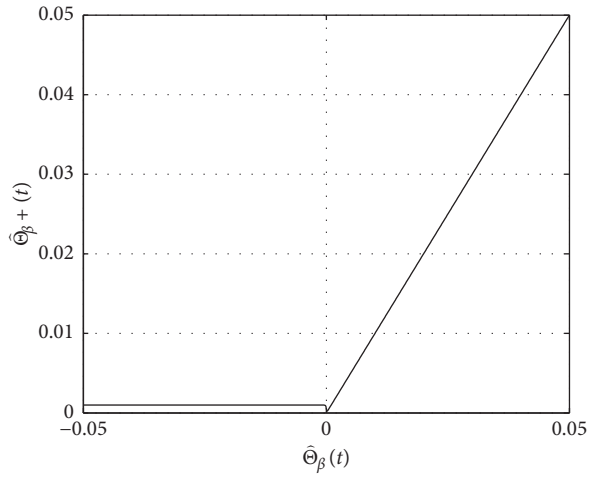

Figure 2: Parametric projection of $\widehat{\theta}_{\beta i+}(t)$.

4.2. Damage Location Algorithm. Assuming that the reference parameters that characterize a nondamage building have been previously estimated or calculated from experiments or material properties, the system identification proposed in the above sections is used to identify real-time parameters that may indicate damage. These parameters are then compared to the nominal parameters in order to locate structural damage. However, an important question in this procedure is how to define an appropriate threshold for damage detection? For this, next, some considerations that must be considered in its design are enumerated:

(a) Taking into account that, for several experiments under the same conditions, results may vary, it is necessary to obtain the average of all involved parameters to obtain a nominal model.

(b) Because structural damage causes changes in all structural parameters, it is necessary to find the maximum change level. This allows to calculate the standard deviation that each parameter may suffer.

(c) Since all the parameters change, the ratio of parameters corresponding to 2 contiguous floors cancels this effect and only occurs when the rate of change is greater than the previously calculated standard deviation.

(d) Finally, due to the damping, which exhibits a random behavior and generally inverses to the wave propagation velocity, the weighted sum of both parameters defines the damage detection threshold.

Therefore, the developed procedure is as follows:

$$\beta_{N_i} = \frac{\widehat{\beta}_{i*}}{\widehat{\beta}_{i+1*}},$$
$$\eta_{N_i} = \frac{\widehat{\eta}_{i*}}{\widehat{\eta}_{i+1*}}, \quad (41)$$
$$i = 1, 2, \ldots, (n-1).$$

For $i = n$,

$$\beta_{N_i} = \frac{\widehat{\beta}_{i*}}{\widehat{\beta}_{i-1*}},$$
$$\eta_{N_i} = \frac{\widehat{\eta}_{i*}}{\widehat{\eta}_{i-1*}}. \quad (42)$$

The relationships between pairs of nominal parameters are obtained.

The relationships between pairs of identified parameters that could indicate damage are also calculated:

$$\beta_{D_i} = \frac{\widehat{\beta}_{di*}}{\widehat{\beta}_{di+1*}},$$
$$\eta_{D_i} = \frac{\widehat{\eta}_{di*}}{\widehat{\eta}_{di+1*}}, \quad (43)$$
$$i = 1, 2, \ldots, (n-1).$$

For $i = n$,

$$\beta_{D_i} = \frac{\widehat{\beta}_{di*}}{\widehat{\beta}_{di-1*}},$$
$$\eta_{D_i} = \frac{\widehat{\eta}_{di*}}{\widehat{\eta}_{di-1*}}. \quad (44)$$

The relative errors between the reference parameters and those possibly indicating damage are computed, i.e.,

$$\varepsilon_{\beta_i} = \frac{\beta_{N_i} - \beta_{D_i}}{\beta_{N_i}} \times 100,$$
$$\varepsilon_{\eta_i} = \frac{\eta_{N_i} - \eta_{D_i}}{\eta_{N_i}} \times 100. \quad (45)$$

The standard deviation of the relative errors is determined by

$$s_\beta = \sqrt{\frac{1}{n-1}\sum_{i=1}^{n}\left(\overline{\varepsilon}_\beta - \varepsilon_{\beta_i}\right)^2},$$
$$s_\eta = \sqrt{\frac{1}{n-1}\sum_{i=1}^{n}\left(\overline{\varepsilon}_\eta - \varepsilon_{\eta_i}\right)^2}, \quad (46)$$

where $\overline{\varepsilon}_\beta = \sum_{i=1}^{n} \varepsilon_{\beta i}/n$ and $\overline{\varepsilon}_\eta = \sum_{i=1}^{n} \varepsilon_{\eta i}/n$ are the mean values of ε_β and ε_η, respectively. Moreover, if the relative error $\varepsilon_{\beta_i} > (\overline{\varepsilon}_\beta + s_\beta)$, $\widetilde{\varepsilon}_{\beta_i} = [\varepsilon_{\beta_i} - (\overline{\varepsilon}_\beta + s_\beta) > 0]$; otherwise, the previous difference is considered null. Similar conditions are applied to values of ε_{η_i}.

Finally, damage is localized using the following expression:

$$S_{dam} = \widetilde{\varepsilon}_{\beta_i} + 1/\widetilde{\varepsilon}_{\eta_i}. \quad (47)$$

Note that when $\widetilde{\varepsilon}_{\eta_i} = [\varepsilon_{\eta_i} - (\overline{\varepsilon}_\eta + s_\eta) < 0]$, a value of $\widetilde{\varepsilon}_{\eta_i} = 10000$ is assigned to prevent indetermination in equation (47). Figure 3 shows the damage detection and localization scheme developed here. This algorithm has the advantage to operate in real time, and therefore, the current condition of structures can be estimated during a seismic action, and an early warning can be issued. Moreover, the damage assessments can be stored and compared, and this information can be useful to decide whether the building should be evacuated, repaired, demolished, or still kept in use.

5. Experimental Results

A five-story building prototype, as shown in Figure 4(a), isused to evaluate the performance of the proposed damage location algorithm. The building is made from aluminum, with the exception of three columns that are made from brass. The dimensions of the columns of the first and the remaining fourth floors are $0.635 \times 0.635 \times 31.5$ cm and $0.635 \times 0.635 \times 36$ cm, respectively. Considering that the first story has an attachment to the base with an height of 4.5 cm, the structure has dimensions of $60 \times 50 \times 180$ cm, and it is mounted on a shaking table actuated by servomotors from Parker, model 406T03LXR, which can be moved in the x-axis and y-axis of the horizontal plane, respectively. However, experiments are based only on the y-axis motion. In addition, the structure is equipped with accelerometers based on MEMS Technologies, model ADXL203E, with a range of ±1.7 g and a bandwidth of [0–50] Hz, which allow to measure absolute acceleration at every story and ground level. Data acquisition was taken using two PCI-6221-M series, electronic boards from National Instruments. Communication between these boards and Simulink were carried out using the Matlab Real-Time Windows Target toolbox. Experiments were executed using a sampling time of 0.001 s.

The North-South component of the 1985 México City earthquake, measured at Secretaria de Comunicaciones y Transportes (SCT), is employed as a source of seismic excitation for the experimental structure. Taking into account the reduced-scale of the building, the amplitude of excitation is adjusted to match with the structure maximum motion, as depicted in Figure 5(a). It is important to note that the used signal has enough richness to identify the structural parameters.

To have preliminary information about the building characteristic, the structure is excited using a chirp signal with a swept-frequency from 0.1 to 15 Hz. The resulting building frequencies are $f_1 = 1.58$ Hz, $f_2 = 4.76$ Hz, $f_3 = 7.51$ Hz, $f_4 = 9.83$ Hz, and $f_5 = 11.51$ Hz, as depicted in Figure 5(b). Considering that the largest frequency is 11.51 Hz, the linear integral filter is designed with a cutoff

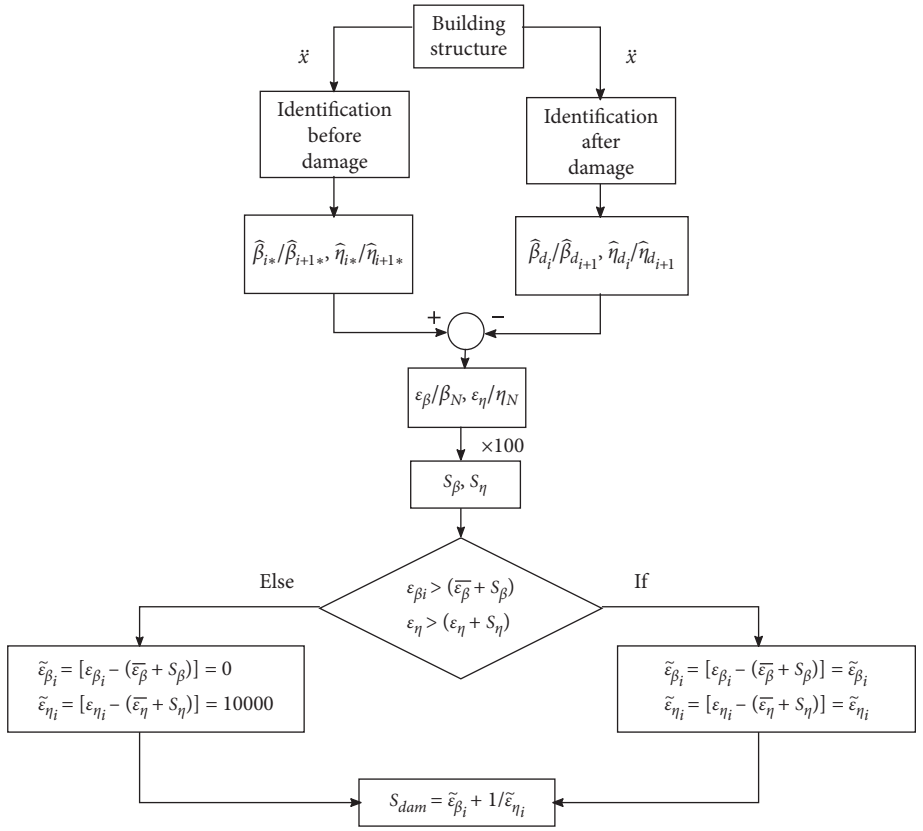

Figure 3: Scheme for damage location.

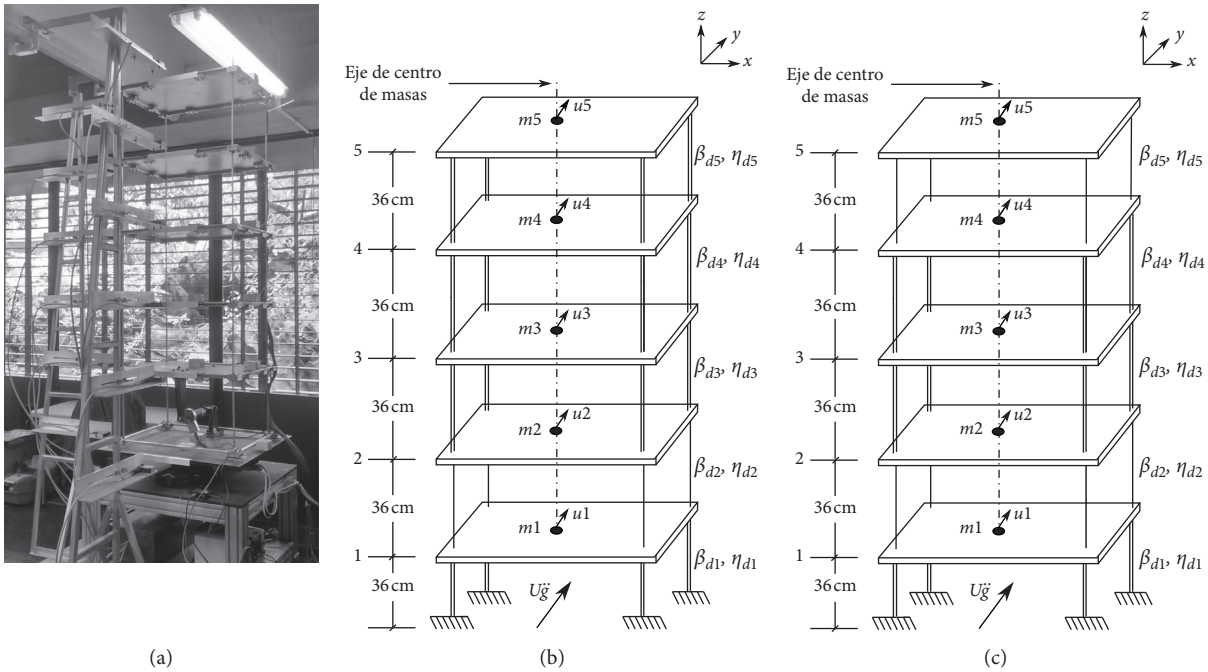

Figure 4: Experimental setup. (a) Scaled five-story building prototype. (b) Building with the presence of damage on the second story. (c) Building with the presence of damage on the second and the fifth story.

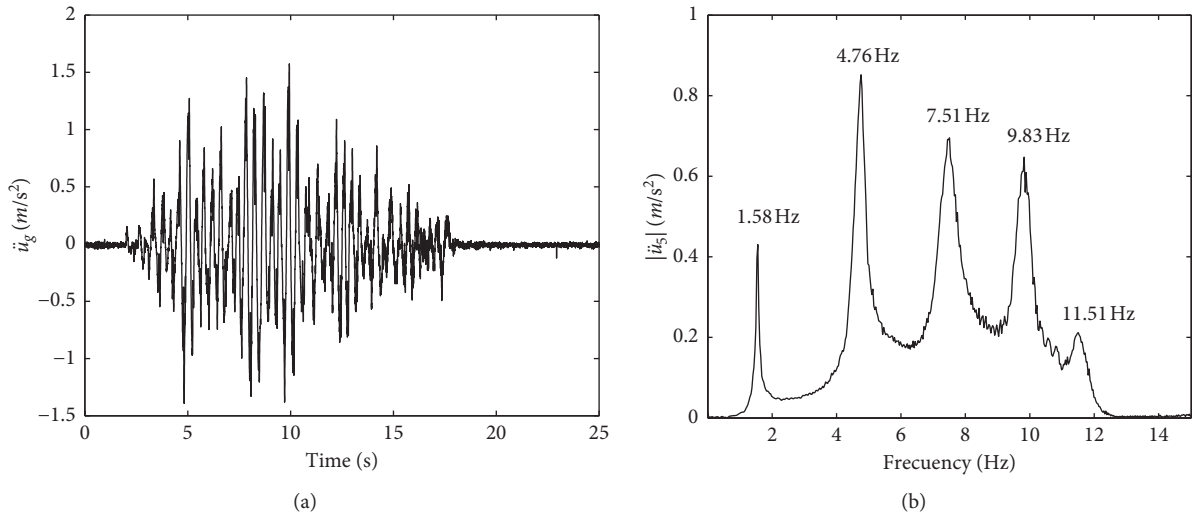

Figure 5: Seismic excitation and structural response bandwidth. (a) Excitation signal: 1985 Mexico City earthquake, North-South component. (b) Vibration frequencies of the building structure.

frequency of 25 Hz to avoid modifying the structural response. Hence, the integration period is $\delta = 0.040$ s, and the integration window length results in $\overline{n} = 40$. The NLSA uses the following parameters; $\alpha = 0.001$ and $P(0) = 10^5 \times I_{(12\times12)}$. For parameter estimation, the building model is discretized at 5 points that match the stories, where acceleration measurement is recorded.

The seismic excitation is applied only at the building-base level, and shear wave velocities and Kelvin damping coefficients are identified for every floor that characterize the nondamage building, as presented in Table 1. From this table, it is clear that the algorithm estimates similar structural properties for floors 2–5, while the first floor differs because its height is slightly smaller than that of other floors, increasing its wave velocity. Evolution of identified parameters is shown in Figures 6(a) and 6(b). However, as real wave velocities and damping coefficients are unknown, they cannot be compared with their estimates. The parameters are validated by comparing the stiffness from the estimated parameters with that obtained from material properties. To carry out this procedure, it is useful to define the following stiffness and damping equations:

$$\widehat{K} = M\beta_{Mr}^2\Lambda_r, \tag{48}$$

$$\widehat{C} = M\eta_{Mr}^2\Lambda_r, \quad \text{with } M = \operatorname{diag}(m_1, m_2, \ldots, m_n). \tag{49}$$

Equations (48) and (49) allow to compute lateral stiffness and damping in the structure. Note that M is a diagonal matrix, where each one of its elements is the mass of the respective story. For the experiments, it was possible to measure each one of these masses that resulted in $m_1 = 10.78$ kg and $m_2 = m_3 = m_4 = m_5 = 9.2$ kg. Table 2 presents the identified lateral stiffness compared with that calculated directly using nominal values of mechanical properties [44], showing that the estimated stiffness is sufficiently close to analytical values on floors 2–5. The first floor is affected by the clamping mechanism increasing its stiffness. In consequence, an error of approximately 5.5% is generated between analytical and estimated stiffness in the worst case. For a real-time experiment, results are considered satisfactory. Damping ratio is more difficult to compare because reference values are not precise [40].

The parameters obtained in this section will be used as reference parameters in the next sections for the purpose of damage detection. For convenience, parameters β_{i*} and η_{i*} are renamed as β_{r_i} and η_{r_i}, while k_i and c_i are renamed as k_{r_i} and c_{r_i}, respectively, where subscript r refers to nominal or reference values.

5.1. Damage Location Task. In this section, the problem of damage detection and location in the five-story reduced-scale building described in the previous section is studied. Here, the building is affected by the presence of damage with two different damage settings: (1) damage at the second story and (2) damage at both second and fifth stories, as in Figures 4(b) and 4(c), respectively. Experiments consist of 2 total tests. In both cases, induced damage was through stiffness loss, and the square cross section of these columns was reduced from of 6.35 to 5 mm, i.e., approximately 23% less with respect to nominal conditions. The intention of this setup controlled experiments is only to ensure a good and appropriate evaluation of the proposed algorithm, with respect to analytical values. Nevertheless, methods under the wave propagation approach are robust to the type and amount of damage, as discussed in [30]. It is important to note that, during experiments, brass and aluminum columns were numbered and referenced at specific positions within the building in order to assure that, after machining, they were replaced in their original position. Moreover, to rebuild the experimental prototype, the torque exerted on the union screws was calibrated to 3 N/m. This helped to guarantee similar conditions for all experiments. Moreover, the 1985

Table 1: Estimated shear wave velocities and Kelvin damping coefficients.

Parameters	Story 1	Story 2	Story 3	Story 4	Story 5
$\widehat{\beta}_{i*}$ (m/s)	13.69	13.31	13.13	13.08	13.05
$\widehat{\eta}_{i*}$ (Nm/s)	0.20	0.21	0.18	0.11	0.07

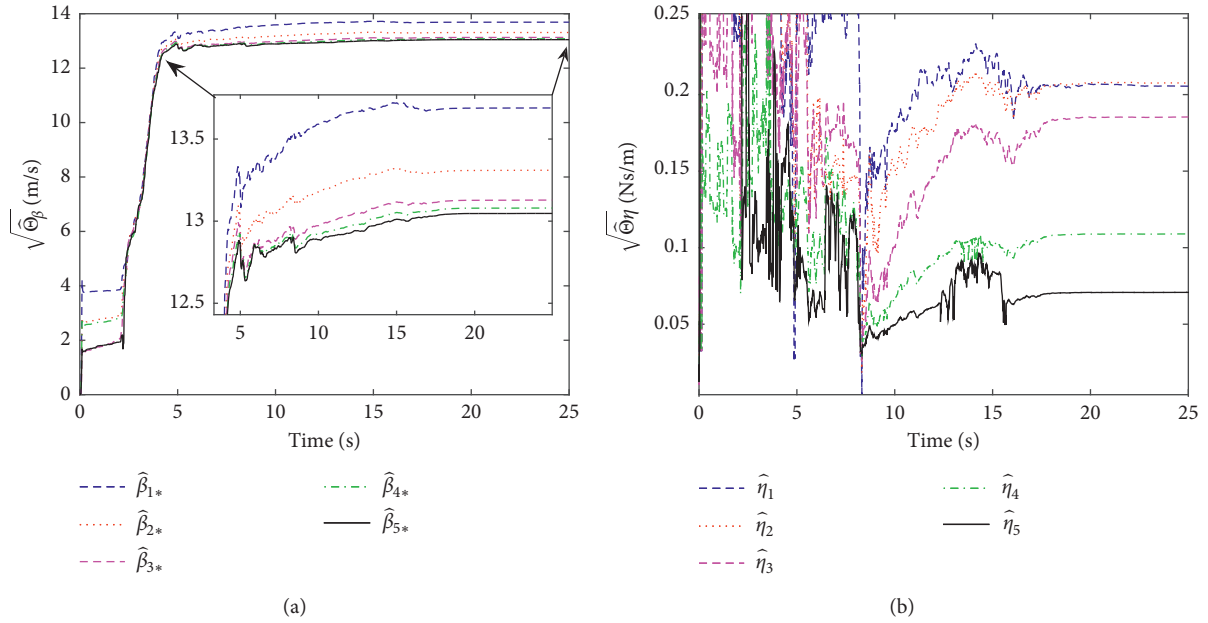

Figure 6: Identified parameters from the discrete shear beam. (a) Evolution of identified $\sqrt{\widetilde{\Theta}_{\beta i+}}$. (b) Evolution of identified $\sqrt{\widetilde{\Theta}_{\eta i+}}$.

Table 2: Comparison between lateral stiffness and estimated stiffness.

Parameters	Story 1	Story 2	Story 3	Story 4	Story 5
k (N/m)	18415.00	12336.00	12336.00	12336.00	12336.00
$\widehat{k}_i$ (N/m)	19406.00	12535.00	12168.00	12026.00	11926.00
$\Delta\widehat{k}/k$ (%)	−5.38	−1.61	1.36	2.51	3.32

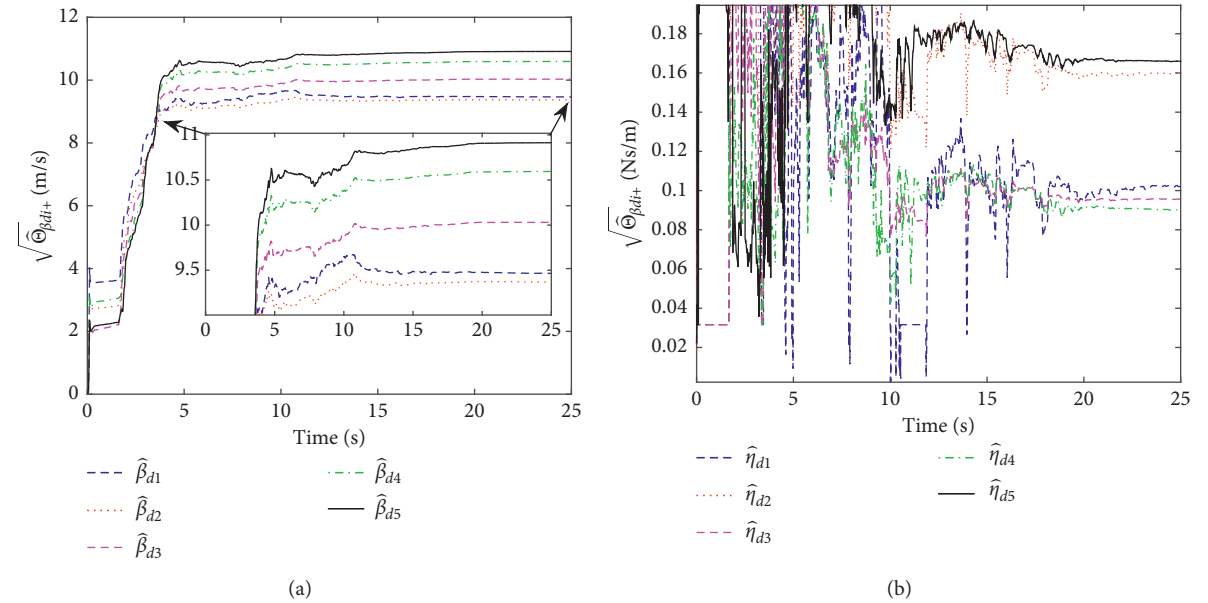

Figure 7: Identified parameters from the damage building at the second story. (a) Evolution of identified $\sqrt{\widetilde{\Theta}_{\beta di+}}$. (b) Evolution of identified $\sqrt{\widetilde{\Theta}_{\eta di+}}$.

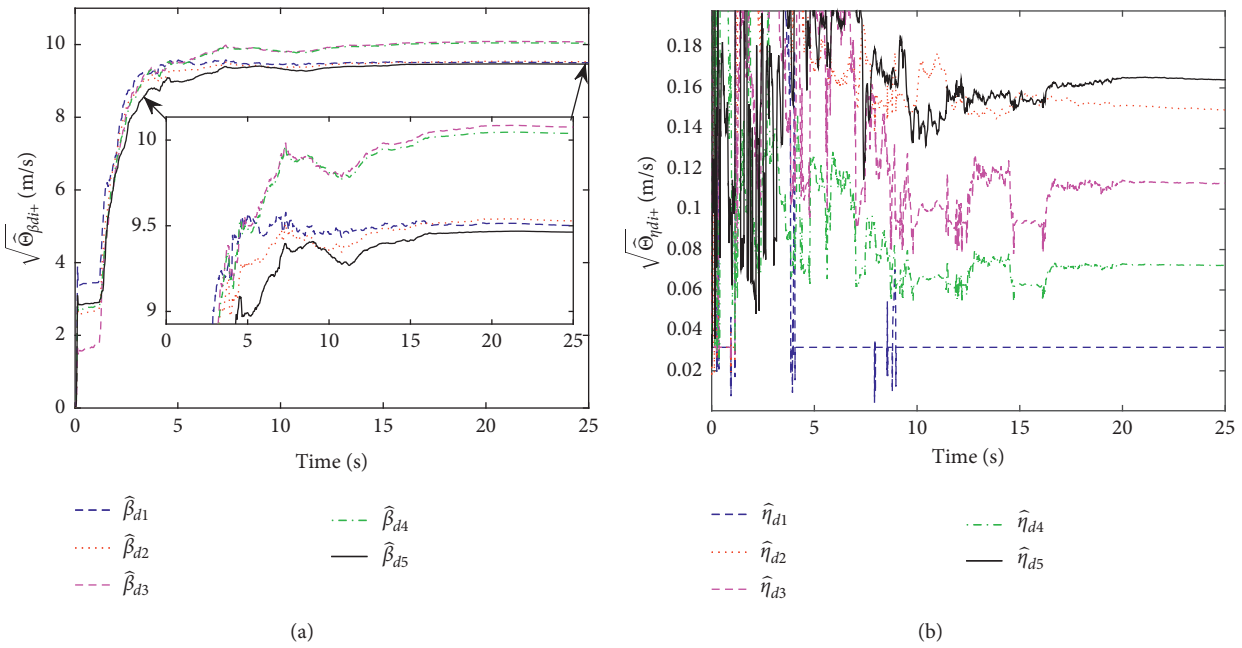

Figure 8: Identified parameters from the damage building at both second and fifth stories. (a) Evolution of identified $\sqrt{\widetilde{\Theta}_{\beta di+}}$. (b) Evolution of identified $\sqrt{\widetilde{\Theta}_{\eta di+}}$.

Table 3: Variation of the estimated parameters β_{di} with the presence of damage.

	$\widehat{\beta}_{d1}$	$\widehat{\beta}_{d2}$	$\widehat{\beta}_{d3}$	$\widehat{\beta}_{d4}$	$\widehat{\beta}_{d5}$	$\widetilde{\beta}_{d1}$ %	$\widetilde{\beta}_{d2}$ %	$\widetilde{\beta}_{d3}$ %	$\widetilde{\beta}_{d4}$ %	$\widetilde{\beta}_{d5}$ %
No damage	13.69	13.31	13.13	13.08	13.05					
Damage on story 2	9.47	9.37	10.03	10.59	10.91	30.83	29.60	23.61	19.04	16.40
Damage on stories 2 and 5	9.50	9.52	10.08	10.04	9.46	30.61	28.47	23.23	23.24	27.51

Table 4: Variation of the estimated parameters η_{di} with the presence of damage.

	$\widehat{\eta}_{d1}$	$\widehat{\eta}_{d2}$	$\widehat{\eta}_{d3}$	$\widehat{\eta}_{d4}$	$\widehat{\eta}_{d5}$	$\widetilde{\eta}_{d1}$ %	$\widetilde{\eta}_{d2}$ %	$\widetilde{\eta}_{d3}$ %	$\widetilde{\eta}_{d4}$ %	$\widetilde{\eta}_{d5}$ %
No damage	0.20	0.21	0.18	0.11	0.07					
Damage on story 2	0.10	0.16	0.10	0.09	0.17	50.0	23.80	44.44	18.18	−142.86
Damage on stories 2 and 5	0.03	0.15	0.11	0.07	0.16	85.0	28.57	38.39	36.36	−128.57

Table 5: Comparison of nominal and estimated frequencies after damage.

	$\widehat{f}_{\mathrm{d1}}$	$\widehat{f}_{\mathrm{d2}}$	$\widehat{f}_{\mathrm{d3}}$	$\widehat{f}_{\mathrm{d4}}$	$\widehat{f}_{\mathrm{d5}}$	$\widetilde{f}_{\mathrm{d1}}$ %	$\widetilde{f}_{\mathrm{d2}}$ %	$\widetilde{f}_{\mathrm{d3}}$ %	$\widetilde{f}_{\mathrm{d4}}$ %	$\widetilde{f}_{\mathrm{d5}}$ %
No damage	1.58	4.76	7.51	9.83	11.51					
Damage on story 2	1.30	3.64	5.79	7.35	8.54	17.72	23.52	22.90	25.22	25.80
Damage on stories 2 and 5	1.22	3.51	5.62	7.20	8.36	22.78	26.26	25.16	26.75	27.36

earthquake, as shown in Figure 5(a), was also used as the seismic excitation for experiments.

Note that the damage produces a decrease in the shear wave velocity and Kelvin damping parameters β_{di} and η_{di} with respect to reference values, as shown in Figures 7(a), 8(a), 7(b), and 8(b), respectively, where subscript d is used to describe parameters obtained with damage presence. Details of these can be found in Tables 3 and 4.

Moreover, vibration frequencies are calculated from estimated parameter matrix $\widehat{\mathscr{A}}$. A comparison between nominal and estimated bandwidths after damage can be found in Table 5. From the results in Table 5, it is clear that all vibration frequencies changed and that the structural response bandwidth is reduced, which is to be expected because damage produces a different structural system in accordance with [4, 5]. This confirms that shear wave velocity and Kelvin damping are successful damage indicators

Table 6: Comparison of nominal and estimated stiffness after damage.

	$\widehat{k}_{d1}$	$\widehat{k}_{d2}$	$\widehat{k}_{d3}$	$\widehat{k}_{d4}$	$\widehat{k}_{d5}$	$\widetilde{k}_{d1}$ %	$\widetilde{k}_{d2}$ %	$\widetilde{k}_{d3}$ %	$\widetilde{k}_{d4}$ %	$\widetilde{k}_{d5}$ %
No damage	19406	12535	12168	12026	11926					
Damage on story 2	7453.3	6211.5	7103.6	7890.0	8344.1	61.59	50.45	41.62	34.39	30.03
Damage on stories 2 and 5	9503.2	6423.1	7167.7	7084.1	6273.6	51.03	48.76	41.09	41.09	47.40

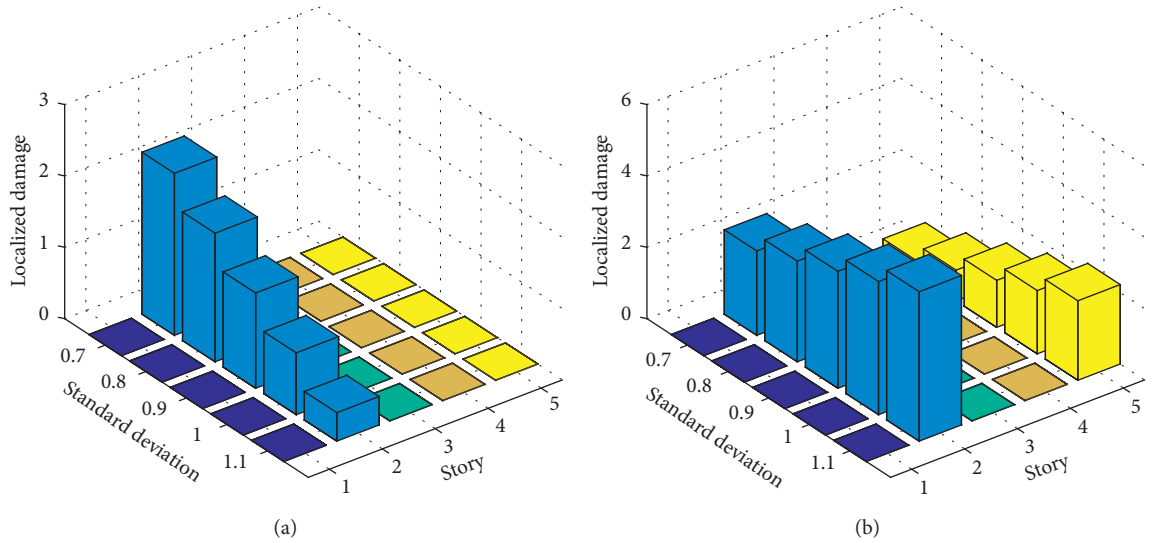

Figure 9: Location and evaluation of structural damage from the damage building. (a) Threshold sensibility analysis, localized damage on story 2. (b) Threshold sensibility analysis, localized damage on stories 2 and 5.

since they are sensitive to structural changes and intrinsically contain information about the damage. On the contrary, considering that the mass-loss in columns is small with respect to the mass of floors, it is valid to assume that the masses here are the same as those of the experiment one without damage, i.e., $m_1 = 10.78\,\text{kg}$ and $m_2 = m_3 = m_4 = m_5 = 9.2\,\text{kg}$. Therefore, the stiffness and damping values are recalculated using equations (48 and 49). Table 6 presents the results in more detail and their comparison with the nominal values.

Despite the information provided by the algorithm, shear wave velocities, Kelvin damping, vibration frequencies, and stiffness values, damage location is still a hard task to realize. For instance, observing results in Table 3, it is evident that the parameters corresponding to the first floor are the most affected because they present a difference of 30.8% between nominal wave propagation velocities and those that identify a damaged behavior. However, considering that the rest of the parameters also changed, it is difficult to assure that damage is located on the first story. For example, the second floor presents a difference of 29% between parameters β_{2*} and $\widehat{\beta}_{d2}$ corresponding to the same level, while on the third floor, there is a difference of 23% for the 2 different damage settings. A similar situation happens analyzing the vibration frequencies and stiffness values presented in Tables 5 and 6, respectively. In contrast to these parameters, the Kelvin damping coefficients presented in Table 4 vary in a random way, and this even more complicates damage location. To overcome these problems, the algorithm proposed in Section 4.2 uses a threshold for the damage location. The simplicity of the method makes it quite promising for real-time applications since no database is needed. Moreover, in order to evaluate the performance of the damage location algorithm, the method developed in Section 4.2 is applied; in addition, a sensitivity analysis is carried out by changing the detection threshold, in particular varying the standard deviation from 70% to 110% of the value calculated in equation (46). Figures 9(a) and 9(b) confirm that the structural damage occurs on floor 2 and then on both floors 2 and 5, for configurations 1 and 2, respectively. The results are still satisfactory varying the standard deviation from 70% to 110%, indicating that the selected damage detection threshold is robust to the threshold selection. All the previous results were obtained using commercial computers.

6. Conclusion

A real-time damage location algorithm based on the wave propagation approach has been presented. Damage location is achieved by using an adaptive detection algorithm and a threshold design scheme that detects changes in the parameters. The threshold has been adjusted to obtain the best performance. The aim is to complement methods based on

the wave propagation approach, which are traditionally developed in the frequency domain and are not suitable for real-time applications. Here, damage is assumed as stiffness loss and is identified by comparing the nominal shear wave velocities and the Kelvin damping coefficients with parameters obtained after a damage occurs. An advantage of the proposed method is the low computing time required for damage detection and location. Since structural parameters are identified in real time, the assessment of structural health can be carried out precisely at the same time. In addition to this, the method can be modified if a more precise location of the damage is desired by placing an additional sensor at the damaged story. Therefore, elements with structural damage can be identified in a specific floor. Furthermore, the proposed method has analytical properties that help to obtain robust results. In fact, the inclusion of linear integral filters in the parameterization removes constant disturbances and attenuates measurement noise from acceleration signals. Moreover, the parametric projection produces stronger convergence properties that improve the identification algorithm. For real-life engineering structures, damage identification, utilizing output-only acceleration measurements, is attractive and promising for practical applications. In this sense, the use of wave methods provides an interesting alternative to modal analysis methods.

We also recognized that it is necessary to carry out more and extensive research to assess the potential of this approach. For instance, damage produced by cracks, cuts, or drilled holes in columns needs to be explored, as well as experiments in x and y coordinates. Nevertheless, the experimental results presented here are a first step in the proper direction. It is convenient to emphasize that the use of controlled experiments ensures a fair and appropriate evaluation of the proposed algorithm, with respect to analytical values. Nevertheless, the proposed wave propagation approach is robust to several types and amounts of damage, as discussed in [30]. At this time, damage quantification is out of the scope of this work, and it is expected to be studied in the near future as structural damage may exhibit nonlinear behavior. This would imply that the amount of damage could not be directly proportional to the estimated wave propagation velocities.

Appendix

A. Bounded and Differentiable Parameters

Led $\widehat{\Theta}_{\beta i+}$ and $\widehat{\Theta}_{\eta i+}$, with $i = 1, 2, \ldots, n$, $\forall t > 0$, be positive and bounded estimated parameters. They are differentiable, and their time derivatives are given by

$$\dot{\widehat{\Theta}}_{\beta i+}(t) = \frac{\dot{\widehat{\Theta}}_{\beta i}(t)}{2}\left[1 + \frac{\chi_1\widehat{\Theta}_{\beta i}(t)}{\sqrt{\left(\chi_1\widehat{\Theta}_{\beta i}(t)\right)^2 + e^2}} - \frac{\chi_1\left(\varsigma_1 - \widehat{\Theta}_{\beta i}(t)\right)}{\sqrt{\left(\chi_1\widehat{\Theta}_{\beta i}(t)\right)^2 + e^2}} + \left(\varsigma_1 - \widehat{\Theta}_{\beta i}(t)\right)\left[\frac{\chi_1^3\widehat{\Theta}_{\beta i}^2(t)}{\left[\sqrt{\left(\chi_1\widehat{\Theta}_{\beta i}(t)\right)^2 + e^2}\right]^{3/2}}\right]\right], \tag{A.1}$$

$$\dot{\widehat{\Theta}}_{\eta i+}(t) = \frac{\dot{\widehat{\Theta}}_{\eta i}(t)}{2}\left[1 + \frac{\chi_2\widehat{\Theta}_{\eta i}(t)}{\sqrt{\left(\chi_2\widehat{\Theta}_{\eta i}(t)\right)^2 + e^2}} - \frac{\chi_2\left(\varsigma_2 - \widehat{\Theta}_{\eta i}(t)\right)}{\sqrt{\left(\chi_2\widehat{\Theta}_{\eta i}(t)\right)^2 + e^2}} + \left(\varsigma_2 - \widehat{\Theta}_{\eta i}(t)\right)\left[\frac{\chi_2^3\widehat{\Theta}_{\eta i}^2(t)}{\left[\sqrt{\left(\chi_2\widehat{\Theta}_{\eta i}(t)\right)^2 + e^2}\right]^{3/2}}\right]\right], \tag{A.2}$$

where $\widehat{\Theta}_{\beta i}(t)$ and $\widehat{\Theta}_{\eta i}(t)$ are provided by the NRLS algorithm. Additionally, variables $\widehat{\Theta}_{\beta i+}(t)$ and $\widehat{\Theta}_{\eta i+}(t) \in \mathscr{L}_2\mathscr{L}_\infty$ because the right-hand side term inside the brackets in equations (A.1) and (A.2) is also bounded. Consequently, $\widehat{A}_{r*}$ is differentiable because this depends on estimated parameters $\widehat{\Theta}_{\beta i}(t)$ and $\widehat{\Theta}_{\eta i}(t)$, which are also positive, bounded, and differentiable, such that $\widehat{A}_{r*} \in \mathscr{L}_2\mathscr{L}_\infty$.

Additionally, since $\widehat{\beta}_M^2$ and $\widehat{\eta}_M^2$ are matrices positive definite matrices $\forall t > 0$ and assuming Λ_r is a diagonally dominant matrix, this ensures that all eigenvalues of matrix $\widehat{A}_{r*}$ have strictly negative real part $\forall t > 0$ such that $\mathrm{Re}\left\{\lambda_i(\widehat{A}_{r*}(t))\right\} < 0$ for each time, where $i = 1, 2, \ldots, 2n$.

B. Notation

Symbols used in this paper are shown in Table 7

Table 7: Symbols used in this paper.

β	Shear wave velociy (m/s)
η	Constant proportional to damping (Ns/m)
u	Displacement (m)
$\dot{u}$	Velocity (m/s)
$\ddot{u}$	Acceleration (m/s^2)
u_g	Ground motion (m)
$\ddot{u}_g$	Ground acceleration (m/s^2)
T	Time (s)
H	Total height of the building (m)
h	Height of the story (m)
Δh	Step of discretization
$\beta_M \Lambda$	Shear wave velocities matrix (m/s)
$\eta_M \Lambda$	Constant proportional to the damping matrix (Ns/m)
Λ	Banded matrix
b	Boundary condition vector
n	Number of floors
I	Identity matrix
ψ	Displacement matrix (m)
$\dot{\psi}$	Velocity matrix (m/s)
$\ddot{\psi}$	Acceleration matrix (m/s^2)
z_m	Acceleration output (m/s^2)
$\beta_v^2 = \Theta_\beta$	Shear wave velocity vector (m/s)
$\eta_v^2 = \Theta_\eta$	Constant proportional to the damping vector (Ns/m)
I_q	Number of integrations over finite time intervals
δ	Size of the moving window
T_s	Sampling time (s)
$\overline{n}$	Length of the time integration window
ψ_β	Filtered displacement signals (m)
ψ_η	Filtered velocity signals (m/s)
Ξ	Filtered acceleration signals (m/s^2)
ϑ	Degree of freedom to normalize the amplitude of the filtered signals
$\dot{P}$	Covariance matrix
α	Forgetting factor
ε	Estimation error
f	Frequencies (Hz)
k	Stiffness (N/m)
C	Damping (Ns/m)
m	Mass of the story (Kg)
ς	Lower bounds for estimated parameters
s_{dam}	Damage story location

Data Availability

Some of the data generated or used during the study are available from the corresponding author upon request.

Conflicts of Interest

The authors declare that there are no conflicts of interest regarding the publication of this paper.

Acknowledgments

The first author was grateful to the Cátedras CONACYT. This research was sponsored by grant UNAM-PAPIIT IT101420.

References

[1] C. H. Jenkins, L. Kjerengtroen, and H. Oestensen, "Sensitivity of parameter changes in structural damage detection," *Shock and Vibration*, vol. 4, no. 1, pp. 27–37, 1997.

[2] Bo Zhao, Z. Xu, X. Kan, J. Zhong, and T. Guo, "Structural damage detection by using single natural frequency and the corresponding mode shape," *Shock and Vibration*, vol. 3, 2016.

[3] E. P. Carden and P. Fanning, "Vibration based condition monitoring: a review," *Structural Health Monitoring: An International Journal*, vol. 3, no. 4, pp. 355–377, 2004.

[4] W. Scott, C. R. Farrar, M. B. Prime, and D. W. Shevitz, "Damage Identification and Health Monitoring of Structural and Mechanical Systems from Changes in Their Vibration Characteristics: Q Literature Review," 1996.

[5] S. W. Doebling, C. Farrar, and M. B. Prime, "A summary review of vibration-based damage identification methods," *The Shock and Vibration Digest*, vol. 30, no. 2, pp. 1–34, 1998.

[6] S. Das, P. Saha, and S. K. Patro, "Vibration-based damage detection techniques used for health monitoring of structures: a review," *Journal of Civil Structural Health Monitoring*, vol. 6, no. 3, pp. 477–507, 2016.

[7] X. Kong, C.-S. Cai, and J. Hu, "The state-of-the-art on framework of vibration-based structural damage identification for decision making," *Applied Sciences*, vol. 7, no. 5, p. 497, 2017.

[8] A. K. Pandey, M. Biswas, and M. M. Samman, "Damage detection from changes in curvature mode shapes," *Journal of Sound and Vibration*, vol. 145, no. 2, pp. 321–332, 1991.

[9] A. K. Pandey and M. Biswas, "Damage detection in structures using changes in flexibility," *Journal of Sound and Vibration*, vol. 169, no. 1, pp. 3–17, 1994.

[10] M. Montazer and S. M. Seyedpoor, "A new flexibility-based damage index for damage detection of truss structures," *Shock and Vibration*, vol. 3, 2014.

[11] H. Sohn, C. R. Farrar, F. M. Hemez, D. Devin, B. R. Nadler, and J. J Czarnecki, *A Review of Structural Health Monitoring Literature: 1996–2001*, Los Alamos National Laboratory, New York, NY, USA, 2003.

[12] H. Sohn and C. R. Farrar, "Damage diagnosis using time series analysis of vibration signals," *Smart Materials and Structures*, vol. 10, no. 3, pp. 446–451, 2001.

[13] K. K. Nair and A. S. Kiremidjian, "Time series-based damage detection and localization algorithm with application to the ASCE benchmark structure," *Journal of Sound and Vibration*, vol. 291, no. 1-2, pp. 349–368, 2006.

[14] O. Abdeljaber, O. Avci, M. S. Kiranyaz, B. Boashash, H. Sodano, and D. J. Inman, "1-D CNNs for structural damage detection: verification on a structural health monitoring benchmark data," *Neurocomputing*, vol. 275, pp. 1308–1317, 2018.

[15] C. Modarres, N. Astorga, E. Lopez Droguett, and V. Meruane, "Convolutional neural networks for automated damage recognition and damage type identification," *Structural Control and Health Monitoring*, vol. 25, no. 10, 2018.

[16] C. R. Farrar and W. Keith, *Structural Health Monitoring: A Machine Learning Perspective*, John Wiley & Sons, New York, NY, USA, 2012.

[17] Y. Bao, C. Song, W. Wang, T. Ye, Lu Wang, and Yu Lan, "Damage detection of bridge structure based on SVM," *Mathematical Problems in Engineering*, vol. 5, p. 2013, 2013.

[18] Y. Zhao, Q. Yan, Y. Zheng, X. Yu, and B. Jia, "A novel artificial bee colony algorithm for structural damage detection," *Advances in Civil Engineering*, vol. 5, p. 2020, 2020.

[19] S. Sehgal and H. Kumar, "Structural dynamic model updating techniques: a state of the art review," *Archives of Computational Methods in Engineering*, vol. 23, no. 3, pp. 515–533, 2016.

[20] J. E. Mottershead and M. I. Friswell, "Model updating in structural dynamics: a survey," *Journal of Sound and Vibration*, vol. 167, no. 2, pp. 347–375, 1993.

[21] S. Sehgal and H. Kumar, "Novel dynamic model updating technique for damped mechanical system," *Journal of Theoretical and Applied Mechanics*, vol. 47, no. 4, pp. 75–85, 2017.

[22] S. Sehgal and H. Kumar, "Damage detection using derringer´s function based weighted model updating method," in *Structural Health Monitoring*, vol. 5, pp. 241–253, Springer, Berlin, Germany, 2014.

[23] S. Sehgal and H. Kumar, "Experimental damage identification by applying structural dynamic model updating," *Journal of Theoretical and Applied Mechanics*, vol. 49, no. 1, pp. 51–61, 2019.

[24] S. Sehgal and H. Kumar, "Damage and damping identification in a structure through novel damped updating method," *Iranian Journal of Sciece and Technology-Transactions of Civil Engineering*, vol. 49, 2020.

[25] G.-H. Kim and Y.-S. Park, "An improved updating parameter selection method and finite element model update using multiobjective optimisation technique," *Mechanical Systems and Signal Processing*, vol. 18, no. 1, pp. 59–78, 2004.

[26] M. D. Kohler, T. H. Heaton, and S. C. Bradford, "Propagating waves in the steel, moment-frame factor building recorded during earthquakes," *Bulletin of the Seismological Society of America*, vol. 97, no. 4, pp. 1334–1345, 2007.

[27] M. Oyunchimeg and H. Kawakami, "A new method for propagation analysis of earthquake waves in damaged buildings: evolutionary normalized input-output minimization (NIOM)," *Journal of Asian Architecture and Building Engineering*, vol. 2, no. 1, pp. 9–16, 2003.

[28] M. D. Trifunac, S. S. Ivanović, and M. I. Todorovska, "Wave propagation in a seven-story reinforced concrete building: III. Damage detection via changes in wavenumbers," *Soil Dynamics and Earthquake Engineering*, vol. 23, no. 1, pp. 65–75, 2003.

[29] M. I. Todorovska and M. D. Trifunac, "Earthquake damage detection in the Imperial County Services Building III: analysis of wave travel times via impulse response functions," *Soil Dynamics and Earthquake Engineering*, vol. 28, no. 5, pp. 387–404, 2008.

[30] M. I. Todorovska and M. T. Rahmani, "System identification of buildings by wave travel time analysis and layered shear beam models-spatial resolution and accuracy," *Structural Control and Health Monitoring*, vol. 20, no. 5, pp. 686–702, 2013.

[31] M. Rahmani and M. I. Todorovska, "1D system identification of buildings during earthquakes by seismic interferometry with waveform inversion of impulse responses-method and application to Millikan library," *Soil Dynamics and Earthquake Engineering*, vol. 47, pp. 157–174, 2013.

[32] M. Rahmani and M. I. Todorovska, "1D system identification of a 54-story steel frame building by seismic interferometry," *Earthquake Engineering & Structural Dynamics*, vol. 43, no. 4, pp. 627–640, 2014.

[33] M. Ebrahimian, M. I. Todorovska, and T. Falborski, "Wave method for structural health monitoring: testing using full-scale shake table experiment data," *Journal of Structural Engineering*, vol. 143, no. 4, 2016.

[34] M. Ebrahimian and M. I. Todorovska, "Structural system identification of building by a wave method based on a nonuniform Timoshenko beam model," *Journal of Engineering Mechanics*, vol. 141, no. 8, pp. 1–31, 2015.

[35] M. I. Todorovska, "Seismic interferometry of a soil-structure interaction model with coupled horizontal and rocking response," *Bulletin of the Seismological Society of America*, vol. 99, no. 2A, pp. 611–625, 2009.

[36] R. Snieder and E. S¸afak, "Extracting the building response using seismic interferometry: theory and application to the Millikan Library in Pasadena, California," *Bulletin of the Seismological Society of America*, vol. 96, no. 2, pp. 586–598, 2006.

[37] J.´S Morales-Valdez, L. Alvarez-Icaza, and A. Concha, "Online adaptive observer for buildings based on wave propagation approach," *Journal of Vibration and Control*, vol. 49, 2017.

[38] N. Fukuwa and S. Matsushima, "Wave dispersion and optimal mass modeling for one dimensional periodic structure," *Earthqueke Engineering and Structural Dynamics*, vol. 23, 1994.

[39] M. Rahmani, M. Ebrahimian, and M. I. Todorovska, "Wave dispersion in high-rise buildings due to soil-structure interaction," *Earthquake Engineering & Structural Dynamics*, vol. 44, no. 2, pp. 317–323, 2015.

[40] A. Chopra, *Dynamics of Structures: Theory and Applications to Earthquake Engineering*, Prentice-Hall, Upper Saddle River, NJ, USA, 1995.

[41] M. Krstic, "Boundary control of PDEs: A course on backstepping designs," *Siam*, vol. 16, 2008.

[42] H. Garnier, M. Mensler, and A. Richard, "Continuous-time model identification from sampled data: implementation issues and performance evaluation," *International Journal of Control*, vol. 76, no. 13, pp. 1337–1357, 2003.

[43] P. Ioannou and J. Sun, *Robust Adaptive Control*, Prentice-Hall, Upper Saddle River, NJ, USA, 1989.

[44] C. Russel, *Mechanics of Materials*, Prentice-Hall, Upper Saddle River, NJ, USA, 8th edition, 2011.